GT4800

Ground Vibration Measurements near Impact Pile Driving

Athina Grizi, S.M. ASCE[1], Adda Athanasopoulos-Zekkos, A.M. ASCE[2] and Richard D. Woods, P.E., D.GE, Dist.M. ASCE[3]

Abstract:

Pile driving is a complex dynamic process where little insight has been garnered in terms of the energy transfer from the driver to the soil and surrounding structures. Ground motion measurements during driving of full scale steel H-piles with diesel hammers are presented. The key feature of this work is the in-depth sensor installation starting very close to the pile (0.2 m), at other radial distances from the pile, and at various depths in the ground. Differences in wave sources from the tip and the shaft of the pile as well as wave attenuation coefficients are revealed from the sensor measurements. Attenuation relationships fitted through the data could be used to predict ground motion that could cause shakedown settlement. A conventional line array of surface mounted geophones was also used and results are presented.

Keywords: Impact Pile Driving; H-Piles; Ground Motion Vibrations; Energy Propagation; Attenuation Rate

[1] Graduate Student, Dept. of Civil and Environmental Engineering, University of Michigan, 2350 Hayward St., Ann Arbor, MI 48109. E-mail: agkrizi@umich.edu

[2] Associate Professor, Dept. of Civil and Environmental Engineering, University of Michigan, 2350 Hayward St., Ann Arbor, MI 48109. E-mail: addazekk@umich.edu

[3] Professor Emeritus, Dept. of Civil and Environmental Engineering, University of Michigan, 2350 Hayward St., Ann Arbor, MI 48109. E-mail: rdw@umich.edu

Introduction and Background

Reports of vibration problems from demolition or construction operations like blasting or pile driving have mainly dealt with direct structural damage from surface waves. Peak particle velocity (PPV) is often considered the measure of vibration intensity to judge direct damage with thresholds of possible damage ranging from 5 to 50 mm/sec (Siskind et al. 1980). A small number of studies have investigated the damage to structures from settlement caused by pile driving or other construction operations. As an example, Lacy and Gould (1985) described damaging settlement from driving H-piles close to a building where the accumulated settlement amounted to 61mm while maximum measured particle velocities on the building were only 2.5 mm/sec. Damaging settlements from vibratory densification (shakedown) of loose sands may occur when shear strain amplitudes exceed the widely accepted threshold of 0.01% (Mohamad and Dobry 1987) even though vibrations on a structure do not exceed the direct damage threshold.

The mechanisms of energy propagation during impact pile driving are complex: spherical waves emanate from the pile tip in the form of body waves (primary waves, P-Waves and shear waves, S-Waves), cylindrical waves radiate from the pile shaft primarily as S-waves, and surface waves (Rayleigh waves, R-waves) propagate along the surface of the ground. Figure 1 illustrates schematically the basic mechanisms of energy transfer to the ground in a uniform soil profile. In a more realistic layered soil profile, the propagation of ground motion is even more complex; reflections and refractions will occur at layer boundaries creating additional waves.

Massarsch (2002) suggested three cylindrical soil behavior zones adjacent to a vertically vibrating compaction pile (Fig. 2) where shear strain (γ) is used to define the boundaries of these zones. Shear strain level can be calculated from the following relationship:

$$\gamma = \frac{\dot{z}}{V_s} \qquad\qquad \text{Eq. 1}$$

where $\dot{z}$ is the peak vertical particle velocity in the soil and V_s is the shear wave velocity. The shear wave velocity increases when moving away from the vibrating source, while the peak vertical particle velocity decreases with increasing distance from the pile as shown schematically in the upper part of Figure 2. The maximum amplitude of soil motion at the pile-soil interface can be estimated by an impedance based equation (Massarsch 2005):

$$\dot{z}_{max} = \frac{\tau}{\rho\, V_s^{*}} \qquad\qquad \text{Eq. 2}$$

where τ is the shear strength of the soil, ρ is the mass density of the soil and V_s^{*} is the shear wave velocity in the soil at large strains. Shear strength and mass density when needed for this equation can be based on standard penetration test (SPT) blow count correlations in the literature.

The attenuation of ground vibrations with distance is often calculated with a formula proposed by Mintrop (1911) and presented by Bornitz (1931):

$$\dot{z}_2 = \dot{z}_1 \left(\frac{r_1}{r_2}\right)^n exp[-\alpha(r_2 - r_1)] \qquad\qquad \text{Eq. 3}$$

where $\dot{z}_1$ and $\dot{z}_2$ are vibration amplitudes at distance r_1 and r_2 from the source, respectively, and α is the attenuation coefficient for a specific soil with the unit for α being 1/distance (1/m). For body waves on a spherical wave front, n=1 while for surface and cylindrical waves n=0.5. The value of the attenuation coefficient depends on the soil type and vibration frequency. Vibrations in soft and/or weak soils diminish rapidly with distance leading to higher attenuation coefficients (Clough and Chameau 1980, Woods 1997).

The California Department of Transportation (2002) indicated that pile driving vibrations attenuate according to the following simple equation:

$$\dot{z}_2 = \dot{z}_1 \left(\frac{r_1}{r_2}\right)^k \qquad\qquad \text{Eq. 4}$$

where $\dot{z}_1$, $\dot{z}_2$, r_1 and r_2 are the same as in Eq. 3 and k is a parameter dependent on soil type but independent of frequency. The k factor includes the material damping of the soil, but does not discriminate between body or surface waves.

In this work, the authors monitored pile driving induced vibrations in close proximity to H-piles driven with diesel hammers to better understand the wave field surrounding the pile. In addition, attenuation curves were fitted to the measured data as an attempt to study how energy diminishes through the soil. A power equation was fitted through the data as a comparison:

$$\dot{z} = a\, r^{-b} \qquad\qquad \text{Eq. 5}$$

where $\dot{z}$ is the vibration amplitude at distance r from the source and a, b are the parameters of the power law.

The initial intent of this research was to study the behavior of various pile driving hammers installing various types of piles. Practical limitations posed by the schedule of construction work by the Michigan Department of Transportation (MDOT) during the term of this research allowed observation of installation of only one type of pile, steel H-piles, driven by only two types of diesel hammers, Pileco D30-32 and Delmag D30-32. The concepts of strain and attenuation presented in Equations 1 to 5 will be employed in the analysis of the ground motions measured in the near vicinity of H-piles driven in sand.

Methodology

Field setup and procedure

Sacrificial sensor packages that could be pushed into the ground with a drill rig and left in the ground after pile driving were developed to record sub-surface ground motion time histories in the three zones surrounding a driven pile (Fig. 2). The sensors were designed to be left in the ground because removing the sensors that had been installed by pushing into position would interfere with operations of the piling contractor. The radial distances of the subsurface sensors from the pile were selected to best define the amplitude decay in the near pile region. Actual distances were picked based on experience of the researchers.

Steel sensor cones 25.4 mm and 31.75 mm in diameter shown in Figure 3 were designed with 60 degrees tapered tips and a hollow cylindrical center to accept motion sensors which were epoxied into place to make them waterproof. Single axis geophones and triaxial Micro-Electro-Mechanical Systems (MEMS) type accelerometers were chosen as the motion transducers (Woods et al. 2014). Economics played an important role in selection and use of sensors since geophones (≈ $35/ea) are relatively inexpensive compared to triaxial MEMS accelerometers (≈ $400/ea).

The cable from the sensors was fed upward through a simple adaptor shown in Figure 3a and 3b which fits the sensor cone to the rod but allows the sensor to be left in the ground when the push rod is withdrawn. The shoulder of the cone that can be seen in Figure 3b and in the inset to Figure 4 was designed with a slightly larger diameter than the drill rod so the shoulder could engage the soil and help withdraw the rod from the cone. This feature of the sensor cone worked in some situations but not in all. In situations where SPT blow counts were less than about 8 (N<8), the sensor cones did not always remain in place as the rod was withdrawn. Other attempts like filling the rods with water and machining a looser fit of the adapter into the drill rods worked in some cases and not in others. The main result of this problem was that sensors were not always installed at the design or optimum elevations in the ground.

Multiple SPT rods of 1.5 m length were used to push the sensor packages to the approximate design depths (Fig. 4). The wires from the sensors were threaded through the hollow core of the drill rod up to the ground surface, where they were connected to the data acquisition system. Voltage output from all sensors was recorded by a multichannel data acquisition system and monitored data were stored in a toughbook computer. More details about the procedure and the sensor cones' fabrication can be found in Athanasopoulos-Zekkos et al. (2013) and Woods et al. (2014).

Monitored Sites

Ground motion during pile driving was monitored at five MDOT sites in Michigan (Fig. 5). Locations were selected where loose, granular, shakedown susceptible soils made up at least part of the soil profile and the sensors were pushed into layers with these characteristics. Sensors were installed and ground motion was measured at different distances from the driven pile in an attempt to differentiate the vibration attenuation in the three soil behavior zones shown in Figure 2 and to accurately characterize the near pile attenuation. Shear wave velocity (V_s) was measured in-situ by the multichannel analysis of surface waves (MASW) technique (Park et al. 1999) at each test site to better understand the dynamic soil stratigraphy of the sites of interest and compare with other available geotechnical characterization. Blow count data was also used to estimate V_s based on correlations in the literature (Imai and Tonouchi 1982) and local correlations based on measurements by MASW.

Results from two of the sites will be presented in the current paper. The MDOT M-139 site was associated with the replacement of a deteriorating river bridge and the MDOT US-131A site involved the construction of a new two-lane bridge over a river. MDOT provided soil profile and

groundwater elevation information based on borings and laboratory tests that were performed for the sites. As shown in Figure 6, the soil profiles for two test borings at the M-139 site consisted of loose sands (SP-SW) to a depth of about 9 m underlain by layers of medium dense to very dense sands (SW) to a depth of about 18 m. The water table was at a depth of about 4.5 m below the surface. The soil profile of the US-131A site consisted of about 6 m of medium dense sand (SW) over a hard sandy clay (CL) to a depth of 12 m and a dense clayey fine sand (SC) to a depth of about 15 m (Fig. 6) and the water level was at about 3 m below the surface.

(a) M-139 site near Niles, MI

A perspective view of sensor locations at the M-139 site near Niles, Michigan is shown in Figure 7. At this site three accelerometers were pushed to a depth of 7.8 m into a layer of loose to medium dense sand at three different radial distances from the pile. Also a line array of surface geophones was placed on the ground with the first instrument (BG1) at 2 m distance from the test pile. A 16.8 m long 360x109 mmxkg/m (14x73 inxlb/ft) H-pile was driven using a Pileco D30-32 diesel hammer. Two geotechnical boreholes were located 1.5 m and 9 m from the pile, TH#4 and TH#1, respectively. The final depth of penetration of the pile was 16.2 m. Two soil profiles for this site are shown in Figure 6 and a composite profile with N and V_s is presented in Figure 8a.

(b) US-131A site near Constantine, MI

Perspective views of sensor locations at the US 131 site near Constantine, Michigan, are shown in Figures 9 and 10. At this site two rows of sensors were pushed to depths of 4.9 m and 10.8 m, respectively at three different distances from the pile. The shallow set of sensors was placed in a loose to medium dense sand layer and the deep set was buried in a hard sandy clay layer (Fig. 9).

Surface geophones for this site were distributed as shown in Figure 10. A 360x109 H-pile of 16.8 m length was driven with a Delmag D30-32 diesel hammer to a depth of 13.1 m. The soil profile, SPT blow counts and V_s for this site are shown in Figures 6 and 8b respectively.

A video was taken during installation of piles at both sites and a detailed analysis followed to determine the number of blows per 0.3 m (1 ft) pile increments. Figures 11a and b show the driving resistance for pile penetration at sites M-139 and US-131A, respectively where the number of blows per 0.3 m is plotted along with the cumulative number of blows versus depth of pile tip.

Ground motion measurements were taken simultaneously at all the sensors and for the whole duration of pile driving at a sampling rate of 1 kHz. All acceleration signals were integrated to velocity for comparison with velocity records from geophones. The plan for controlling orientation of the two horizontal directions depended on keeping the push rods alignment constant with continual visual observation at the surface. It became evident during installation of the sensors that this approach was too crude for accurate orientation control. It was also observed that the amplitudes of the horizontal motion components were less than 30% of the vertical motion. For these reasons only vertical ground motions are presented here.

Analysis of Results

Ground Motion Measurements

The ground motion measurements are presented in terms of vertical peak particle velocities ($\dot{z}$) versus pile tip elevation. Figure 12 compares vertical peak particle velocities ($\dot{z}$) at the buried sensors, at three distances from the pile at the M-139 and US 131A sites. The maximum particle velocity per 0.3 m increments of depth was extracted and is plotted at the mid-depth of each pile penetration increment (per ft). As expected, the sensors closest to the pile (A3, A1, and A2

respectively) have the highest ground motion amplitudes. The horizontal lines in Figures 12a, b, c indicate the common depth of the transducers.

In all cases, when the pile tip is above the sensor, the ground motion amplitudes slowly increase with pile tip depth. As the pile tip reaches the depth of the sensors, there are greater increases in particle velocities and the behavior is more intense for the sensor closest to the pile face. This observation is consistent with the fact that the sensor can only sense the waves coming from the tip of the pile by body waves when the tip is still above the instrument. Both tip and shaft waves are captured by the sensor when the tip reaches and passes the sensor depth.

The surface geophones, as expected, recorded lower velocities than embedded sensors at both sites, as can be seen by comparing particle motion amplitudes in Figures 12 (at-depth) and 13 (on-surface). An interesting comparison can be made by looking at sensors BG1 and A5 for both sites, Figure 14a and b. These two sensors were located at the same radial distance (2m) from the driven pile; BG1 was placed on the surface while A5 was pushed into the ground at 7.8 m and at 4.9 m at the M-139 site and at the US-131A site, respectively. The comparison shows that below ground and surface motions at a distance of 2 m from the pile have similar trends until the pile tip passes the depth of the sensor. At greater pile tip depths, the relationship becomes more complicated with the below ground motions having a tendency to be greater than surface motions.

Another way of presenting the ground motion data is shown in Figures 15, 16 and 17. The diagonal distance (resultant of vertical and horizontal distances) from pile tip to the in-depth sensor location versus the vertical peak particle velocity, is plotted for each sensor for both sites in these figures. The solid symbols represent data collected when the pile tip was above the elevation of the sensor while the open symbols represent data collected when the pile tip was below the elevation of the sensor. As the pile tip goes deeper and closer to the depth of the sensor during

driving the diagonal distance decreases and the ground vibration amplitudes increase. When the tip reaches the elevation of the sensor and then goes below (diagonal distance increasing), the velocity data are either almost constant or rise before falling off when the tip is far from the sensor. This behavior is most evident for the sensors closest to the pile, A3 for the M139 site and A1, A2 for the US-131A site.

Wave Attenuation

Attenuation of the pile driving induced sub-surface vibrations for the M-139 site are shown in Figure 18a. The vertical peak particle velocity was plotted versus sensor distance from pile for each common sensor depth. Coefficients of attenuation, α, were determined by fitting Eq. 3 with n=0.5 through alternate pairs of recorded pulses when the pile tip was at the depth of the sensors (7.8 m). The α values are collected in Table 1 and averages are shown on Figure 18a. An average value of α=0.36 (1/m) from these three pairs of calculations was used to plot the α attenuation curve shown on Figure 18a. The sensor closest to the pile (A3) was the base from which the curve is drawn. The ground motion at the pile-soil interface was calculated as 457 mm/sec using Eq. 2 where a radial distance of 0.03 m from the center of the H-pile was used to represent the pile-soil interface.

In a similar way, attenuation parameters k were calculated by fitting Eq. 4 through pairs of ground motion data (Table 1) with the average value of k=0.69 used to plot the k decay curve in Figure 18a. Finally, a power equation, Eq. 5, was fitted through data points from sensors A3, A4 and A5 for comparison.

An attenuation curve of vertical peak particle velocity is presented in Figure 18b for the surface geophones at the M-139 site with the maximum amplitude of each instrument selected and

plotted when the pile was being driven from 3.7 m to 4.0 m depth. Eq. 3 with n=0.5 was used to derive an average coefficient of attenuation of 0.13 (1/m) as shown in Figure 18b. The curve was drawn using as reference point the value of the geophone closest to the pile (BG1).

Table 2 presents attenuation coefficients, α and k, calculated by fitting Eq. 3 and 4 through pairs of values of the three sensors, located at the shallow depth, for site US-131A. Similar results are shown in Table 3 for the deep set of sensors at the same site. In Figure 19a, the attenuation curves for the sensors buried at a shallow depth (loose to medium sand) were plotted using the average values of α=0.58 (1/m) and k=0.82 with the amplitude from A1 sensor used as the reference point. The ground motion amplitudes for sensors A1, SG1 and A5 were extracted when the pile was being driven from 5.5 m to 5.8 m depth. The maximum particle vibration velocity at the pile-soil interface is predicted from Eq. 2 as 559 mm/sec at a distance of 0.03 m from the pile. Figure 19b presents attenuation relations with data from the sensors that were pushed to a final depth of 10.8 m (hard sandy clay layer). Maximum amplitudes were selected for every transducer when the pile was being driven from 10.4 m to 10.7 m. The maximum particle vibration velocity at the pile-soil interface was estimated as 605 mm/sec. Average values of α=0.54 (1/m) and k=0.95 were chosen to fit the monitored data where A2 sensor was the base point for the drawn curve. The power equation, Eq. 5, is again shown for comparison. Also, in Figure 19c the decay Eq. 3 with n=0.5 was fitted through ground surface vibration data measured on the surface with six geophones; BG1 was the base point to draw the curve. The data shown were selected when the pile was penetrating from 3.1 m to 3.4 m. The average attenuation coefficient was found to be 0.13 (1/m).

Discussion of results

Ground Motion Measurements

Records from the in-depth sensors provided valuable information on energy propagation through the ground during impact pile driving. Vibration measurements at the MDOT sites generally support the hypothesis of energy transfer from pile to soil as suggested in Figure 1. It is shown in Figures 15 to 17, that ground motion increases as the diagonal distance from pile tip to sensors decreases when the pile tip is above the depth of the sensor (read data points from lower right upward to the left to visualize this representation in Fig. 15). During this reach of pile driving, it is primarily spherical body waves from the pile tip that impact the sensors. Cylindrical waves from the pile shaft do not travel on paths that encounter the sensors in this driving reach. After the pile tip passes the depth of the sensor, both spherical waves from the pile tip and cylindrical waves from the pile shaft impact the sensors and the ground motion amplitude remains nearly constant until the pile tip is at considerable distance from the sensor (Fig. 15). All these observations are most clearly representative at the sensors closest to the pile, and as such, support the wave propagation hypotheses shown in Figure 1.

The increase in amplitude around 10.7 m and the slight increase around 13.7 m in Figure 12a, should be attributed to the higher driving resistance at these depths as depicted in Figure 11a. SPT values increase at 10.7 m according to TH#4 and at 13.7 m according to TH#1 (Fig. 8a), which indicates again that the resistance is greater, therefore higher vibration levels are monitored by the three accelerometers. The trend is more evident for the sensor located nearest to the pile (A3).

Except for very shallow soil depths, where local disturbance may change the character of the ground, the amplitude of ground motion decreases with increasing distance from the pile as expected (Fig. 12a). The small spike in the signal around 3.1 m diagonal distance (Fig. 15)

represents the change in driving resistance at 10.7 m depth where the character of the soil has changed significantly. Ground motion records from the surface geophones (Fig. 13a) show a similar vibration pattern; the further the sensor from the pile the smaller the peak particle velocities. There is an increase in velocity amplitudes in all four surface geophones when the pile tip is between 4.9 m and 6.5 m as the pile penetrates into the hard clayey silt layer and the driving resistance increases.

Similar trends are observed by examining the data from US-131A site where two rows of sensors were installed in the sub-surface. As shown in Figure 9, three sensors were placed in the shallow loose to medium sand layer and three were pushed into the hard sandy clay layer. Inspection of the ground motion data of the set of sensors in Figures 12b and c, reveals that the vertical peak particle velocities follow the behavior of M-139 site; the shaft contribution is evident when the pile has passed the elevation of the sensors. In addition, at 6.1 m depth the SPT blow counts increase as the pile enters into the hard clay layer (Fig. 6), which results in an increase of the particle velocity amplitudes (most obvious in the two closest sensors from the pile, A1 and SG1, Fig. 12b). In Figure 16, where the diagonal distance from the pile tip is plotted versus the vertical peak particle velocity, it is evident that when the pile descends below the elevation of the sensors, the amplitudes first increase, reach a plateau and then decrease (noticeable in two closest sensors to the pile, A1 and SG1). The influence of the cylindrical waves from the shaft added to the spherical waves emanating from the tip increase the vibration levels, but when the pile moves deeper the effect from the body waves starts to decrease and the sensors at the shallow depth principally record S-waves coming from the pile shaft. Similar trends can be observed by examining the data from the deep sensors (Fig. 17).

Ground motions from the six surface geophones shown in Figure 13b show that at 6.1 m depth of penetration the vertical ground motion increased in all sensors. This behavior is most likely attributed to impedance mismatches and reflections and refractions of the waves at the layer boundaries, and are beyond the scope of the current paper. There is a significant increase of vibration velocity at 7.8 m depth, captured by the two closest geophones to the pile (BG1 and BG2), however, an analogous increase to the penetration resistance or to the SPT blow counts was not observed.

Wave Attenuation

The below-ground motion amplitude reduction as characterized by Equations 3 and 4 and shown in Figures 18 and 19 shows very good fit. Tables 1 to 3 summarize the attenuation coefficients resulting from these analyses along with averages and statistical R-square values. The calculated attenuation coefficients, α, for both sites when the pile tip is in the sand layer (Tables 1 and 2), show a high rate of attenuation close to the pile face; α is 0.71 and 1.14 (1/m) when fitting Eq. 3 to the closest pair of sensors to the pile for site M-139 (A3 and A4) and US-131A (A1 and SG1), respectively. This rate decreases dramatically when moving away from the pile; alpha coefficients are one order of magnitude less when fitting Eq. 3 to the furthest two sensors for both sites. This behavior is in agreement with the hypothesis presented in Figure 2 where ground motion amplitude is shown to decrease at a decreasing rate as distance from the pile increases. It is of interest to investigate the behavior of the sensors that were pushed in the clay layer at US-131A site. Here, the α value calculated in Table 3 for the closest pair of sensors to the pile (A2 and A4) is not high compared to the α found for the sand layer, however, there is still a high rate of attenuation for points A4 and SG2 which are further away from the pile (Table 3). Therefore, by comparing the

data from the two sets of sensors in the sand and clay layers at US-131A, the monitored amplitudes of ground motion were significantly higher when the pile was driven in the clay layer but vibrations decayed more rapidly with distance than those in the sand layer. Similar comments can be made for the k coefficients calculated by fitting Eq. 4 to the recorded data. It should be noted that the estimated ground motion from Eq. 2 at the pile-soil interface, is very close to the back-calculated value of the attenuation curves using Eq. 3 and 4 for both sites (Fig. 18a, 19a and 19b).

Surface wave attenuation coefficients, α, obtained at the M-139 and US-131 MDOT sites are close to those determined by other researchers. Attenuation coefficients from this study were calculated as 0.13 (1/m) for both sites as shown in Figs. 18b and 19c. Woods (1997) suggested an average alpha coefficient of 0.07 (1/m) for a sandy soil with SPT blow count of 10 and a frequency of 25 Hz. Most blows from the current work had dominant frequencies around 25 Hz. Kim and Lee (2000) measured vibration data on the surface while driving a steel pipe pile of 0.6 m diameter in similar soil conditions and the alpha coefficient was calculated as 0.03 (1/m) with a frequency around 10 Hz.

Extensive analysis of the dominant frequency content of ground motion at both sites resulted in a range of dominant frequencies between 25 and 150 Hz. The high frequency of the impact from the hammer diminishes as it travels from the top to the tip of the pile, and further reduction in the dominant frequency content occurs as the wave propagates into the soil mass (Hajduk et al. 2000, Thandavamoorthy 2004). This trend can be seen in Figures 20a and b where examples of a time history along with the frequency domain of a single blow are presented for two sensors at the M-139 site, A3 and A4, located at different distances from the pile, where high frequencies in the 100 to 200 Hz range have diminished as waves travel from sensor A3 (0.2 m from pile) to sensor A4 (0.8 m from pile).

Conclusions

The hypotheses describing energy dissipation in the ground surrounding the impact driving of H-pile in loose sand have been qualitatively confirmed by monitoring ground motion at the ground surface, in-depth and in radial distance from the pile at two sites provided by MDOT. Those measurements qualitatively demonstrate the dissipation of pile driving energy through the ground through two main types of energy transmission, spherical body waves from the pile tip and cylindrical shear waves from the pile shaft. While specific strain levels have not been determined for the three suggested zones of attenuation, the concept of decreasing rates of attenuation with increased distance from the source has been confirmed. Both frequency based and power based attenuation relationships were demonstrated to be valid and calculated surface wave attenuation coefficients were similar to those in the literature.

In a future publication, the ground motion amplitude and attenuation data from these tests are to be converted to shear strain amplitude to judge potential for exceedance of threshold strain and subsequent ground settlement (shakedown settlement).

References

Athanasopoulos-Zekkos, A., Woods, R.D. and Grizi, A. (2013), "Effect of Pile-Driving Induced Vibrations on Nearby Structures and Other Assets," Final Report to Michigan Department of Transportation, ORBP Number OR10-046, November 2013.

Bornitz, G. (1931), "Uber die Ausbreitung der von Groszkolbenmaschinen erzeugten Bodenschwingungen in die Tiefe", J. Springer (Berlin).

California Department of Transportation (2002), "Transportation Related Earthborne Vibrations (Caltrans Experiences)", Technical Advisory, Vibrations, TAV-02-01-R9601, Prepared by Rudy Hendriks, 33 pp.

Clough, G.W. and Chameau, J.L. (1980), "Measured Effects of Vibratory Sheetpile Driving", Journal of the Geotechnical Engineering Division, ASCE, Vol. 106, No. GT10, October 1980, pp. 1081 1099.

Hajduk, E.L. Paikowsky, S.G., Hölscher, P, and van der Pool, T. (2000), "Accelerations of a Driven Pile and the Surrounding Soil", Proceedings of the 6th International Conference on the Application of Stress-Wave Theory to Piles, September 11 13, 2000, Sao Paulo, Brazil, pp. 541 548.

Imai, T. and Tonouchi, K. (1982), "Correlation of N Value with S-Wave Velocity and Shear Modulus", Proc. Of 2nd European Symposium on Penetration Testing, Amsterdam, pp. 67-72.

Kim, D.S. and Lee, J.S. (2000), "Propagation and attenuation characteristics of various ground vibrations", Soil Dynamics and Earthquake Engineering, Vol. 19, pp. 115 126.

Lacy, H.S. and Gould, J.P. (1985), "Settlement from Pile Driving in Sands", Proceedings of a Symposium sponsored by the Geotechnical Engineering Division in conjunction with the ASCE Convention in Detroit, Michigan, October 1985, pp. 152 173.

Massarsch, K.R. (2002), "Effects of Vibratory Compaction", TransVib 2002 – International Conference on Vibratory Pile Driving and Deep Soil Compaction, Louvain-la-Neuve, Keynote Lecture, pp. 33 42.

Massarsch, K.R. (2005), "Ground Vibrations Caused by Impact Pile Driving", Invited Lecture, Proceedings, Environmental Vibrations: Prediction, Monitoring, Mitigation and Evaluation (ISEV 2005). Okayama University, Japan, 20 - 22. September 2005. Taylor & Francis. pp. 369 379.

Mintrop, L. (1911), "Uber die Ausbreitung der von den Massendrucken einer Grossasmaschine erzeugten Bodenschwingungen", Dissertation Gottingen.

Mohamad, R. and Dobry, R. (1987), "Settlements of cohesionless soils due to pile driving", Proceedings, 9th Southeast Asian Geotechnical Conference, Bangkok, Thailand, pp. 7-23 – 7-30.

Park, C.B., Miller, R.D., and Xia, J. (1999), "Multichannel analysis of surface waves", Geophysics, v. 64, pp 800 – 808.

Siskind D.E., Stagg M.S., Kopp J.W. and Dowding C.H. (1980), "Structure Response and Damage Produced by Airblast from Surface Mining", U.S. Bureau of Mines, RI 8507.

Thandavamoorthy, T.S. (2004), "Piling in fine and medium sand – a case study of ground and pile vibration", Soil Dynamics and Earthquake Engineering, Vol. 24, pp. 295 – 304.

Woods, R.D. (1997), "Dynamic Effects of Pile Installations on Adjacent Structures", Synthesis of Highway practice 253, National Cooperative highway research program, Washington, D.C., 1997.

Woods, R.D., Athanasopoulos-Zekkos, A., Gkrizi, A., Pietrangelo, A. and Zimmerman, A. (2014), "Measurement of Ground Motion near Piles during Driving", ASCE, Geotechnical Special Publication (GSP) No. 233, From Soil Behavior Fundamentals to Innovations in Geotechnical Engineering: Honoring Roy E. Olson, pp. 512 – 521.

List of Figures

Table 1. Coefficients of attenuation for sensors at M-139 site

M-139	Distance from pile (m)	$\dot{z}$ (mm/sec)	Sensor Depth 7.8 m	α (1/m)	k
PILE	0.03	457.2			
A3	0.15	121.7	**A3-A4**	0.71	0.77
A4	0.76	35.3	**A4-A5**	0.08	0.61
A5	1.98	19.8	**A3-A5**	0.29	0.71
			average	**0.36**	**0.69**
			R²	0.988	0.997

Table 2. Coefficients of attenuation for shallow sensors at US-131A site

US-131A	Distance from pile (m)	$\dot{z}$ (mm/sec)	Sensor Depth 4.9 m	α (1/m)	k
PILE	0.03	558.8			
A1	0.15	150.4	**A1-SG1**	1.14	0.95
SG1	0.82	30.1	**SG1-A5**	0.12	0.65
A5	2.04	16.6	**A1-A5**	0.48	0.85
			average	**0.58**	**0.82**
			R²	0.983	0.995

Table 3. Coefficients of attenuation for deep sensors at US-131A site

US-131A	Distance from pile (m)	$\dot{z}$ (mm/sec)	Sensor Depth 10.8 m	α (1/m)	k
PILE	0.03	604.5			
A2	0.15	247.4	**A2-A4**	0.43	0.66
A4	0.76	84.9	**A4-SG2**	0.62	1.29
SG2	1.98	24.7	**A2-SG2**	0.56	0.90
			average	**0.54**	**0.95**
			R²	0.998	0.960

1

2   Fig. 1

	Shear Strain $\gamma < 10^{-3}$ %	Shear Strain 10^{-3} % $< \gamma < 10^{-1}$ %	Shear Strain $\gamma > 10^{-1}$ %
M-139	$\alpha=0.08$	$\alpha=0.29$	$\alpha=0.71$
US-131A	$\alpha=0.12$	$\alpha=0.48$	$\alpha=1.14$
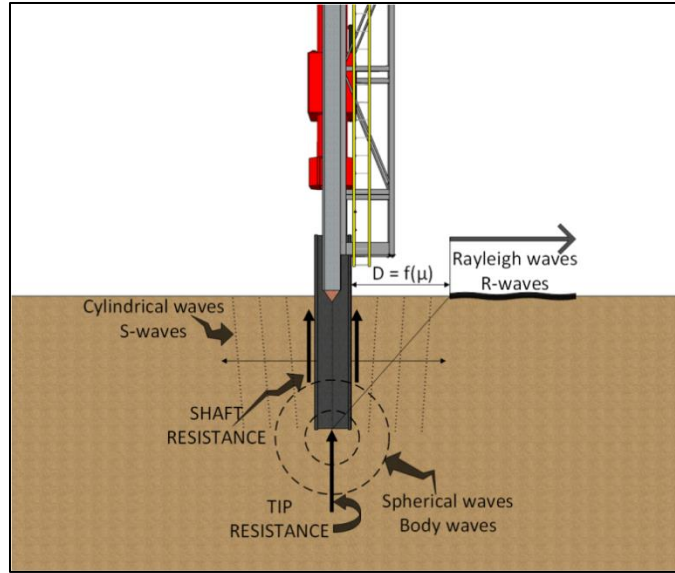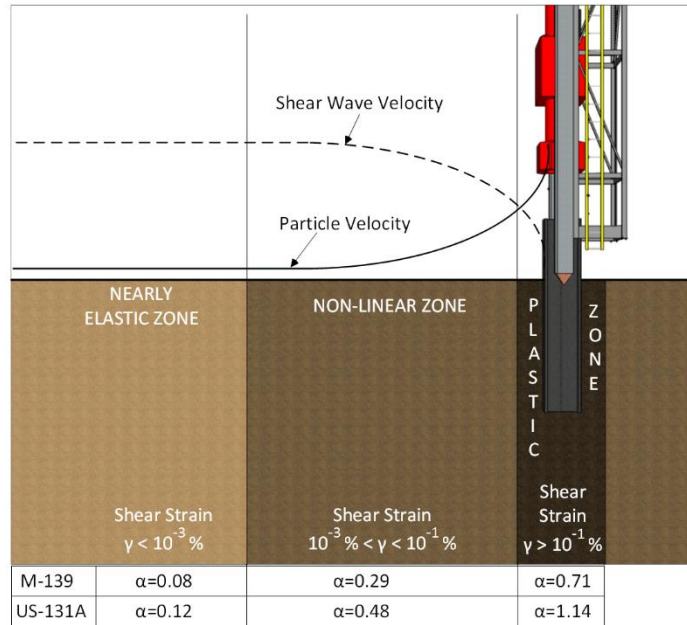
3

4   Fig. 2

5

6   Fig. 3(a); (b)

7

8   Fig. 4

9

Fig. 5

11

Fig. 6

13

Fig. 7

15

Fig. 8 (a); (b)

17

Fig. 9

19

Fig. 10

21

Fig. 11 (a); (b)
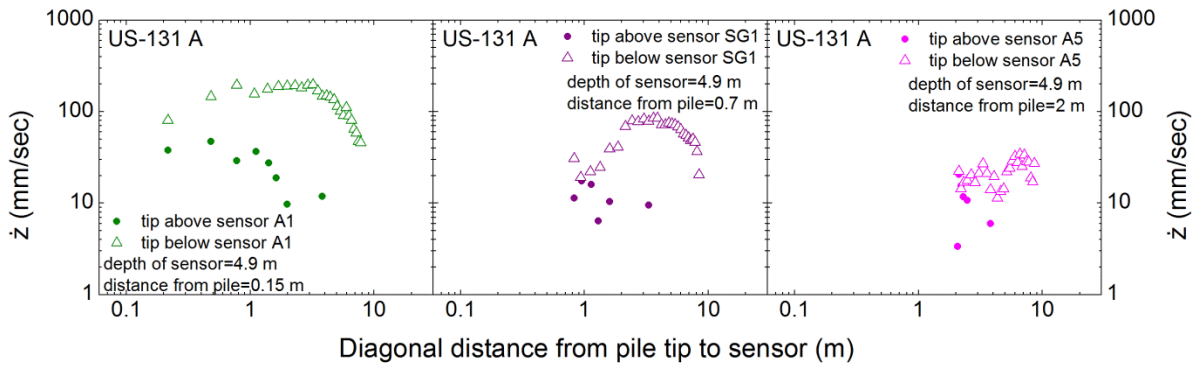
22

23

Fig. 12 (a); (b); (c)
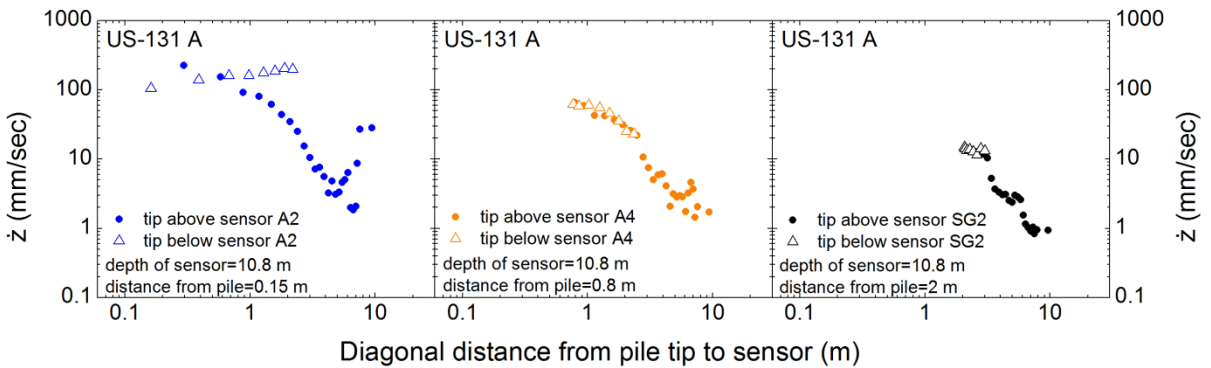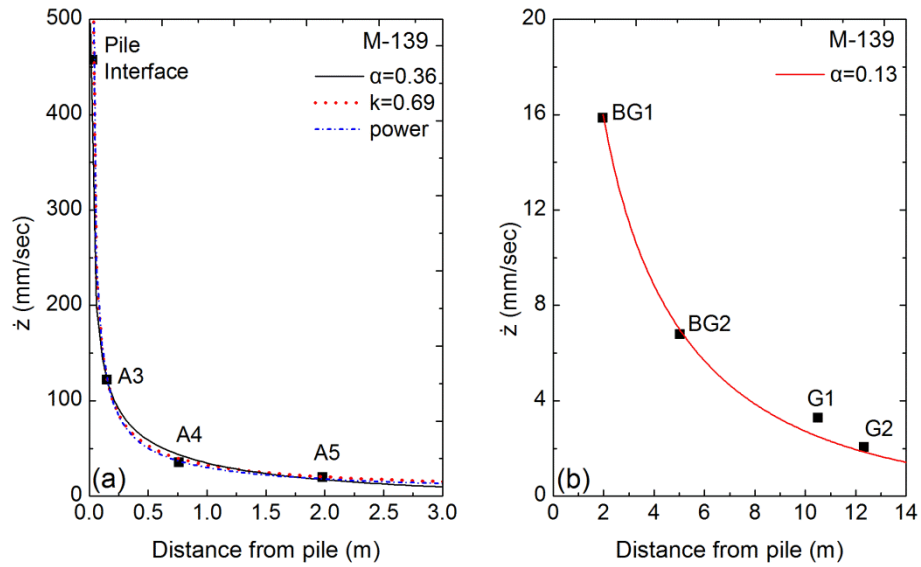
24

25

26

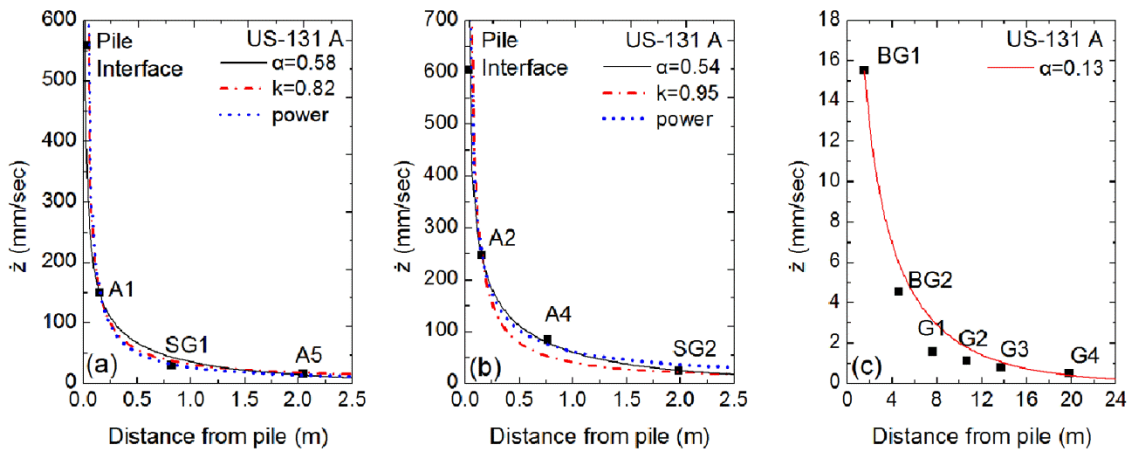27 Fig. 13 (a); (b)

28

29 Fig. 14 (a): (b)

30

31

Fig. 15

33

Fig. 16

35

Fig. 17

37

Fig. 18 (a); (b)

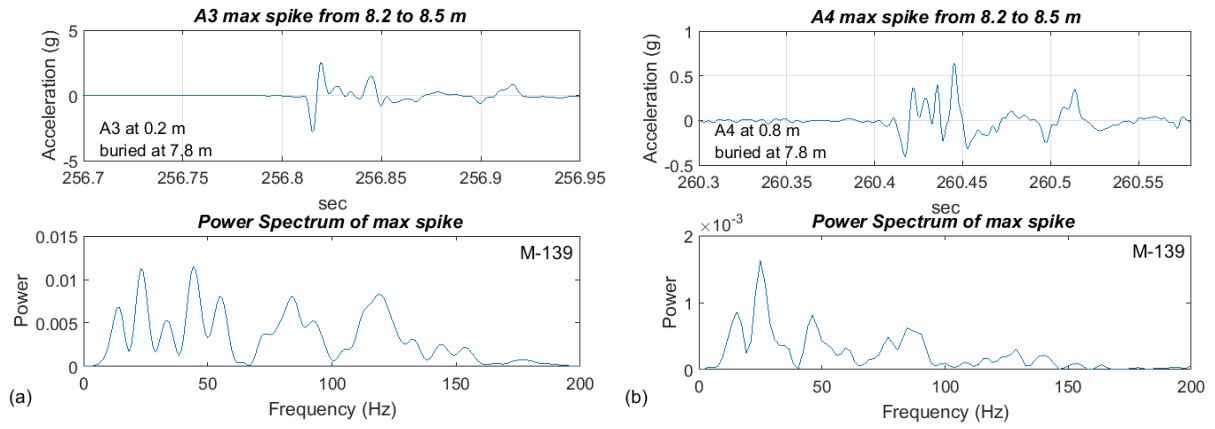39

Fig. 19 (a); (b); (c)

41

42

43

44

A3 max spike from 8.2 to 8.5 m

A3 at 0.2 m
buried at 7.8 m

Power Spectrum of max spike

M-139

A4 max spike from 8.2 to 8.5 m

A4 at 0.8 m
buried at 7.8 m

Power Spectrum of max spike

M-139

(a)

(b)

45

46   Fig. 20(a); (b)

47

48

49